Advances in Materials Physics and Chemistry, 2018, 8, 246-256
http://www.scirp.org/journal/ampc
ISSN Online: 2162-5328
ISSN Print: 2162-531X

Discovery of β-HIO_3: A Metastable Polymorph of HIO_3

Dylan K. Smith[1], Daniel K. Unruh[2], Michelle L. Pantoya[1]

[1]Department of Mechanical Engineering, Texas Tech University, Lubbock, USA
[2]Department of Chemistry, Texas Tech University, Lubbock, USA
Email: michelle.pantoya@ttu.edu

How to cite this paper: Smith, D.K., Unruh, D.K. and Pantoya, M.L. (2018) Discovery of β-HIO_3: A Metastable Polymorph of HIO_3. *Advances in Materials Physics and Chemistry*, **8**, 246-256.
https://doi.org/10.4236/ampc.2018.85016

Received: April 11, 2018
Accepted: May 28, 2018
Published: May 31, 2018

Abstract

The β-HIO_3 polymorph, previously difficult to detect and whose existence was questioned, has been structurally characterized. The crystal structure of β-HIO_3 was solved in the same space group as α-HIO_3 (P212121); however, it was found that the unit cell axes were all different by about 1 Å. Similar to that of α and γ phases, the unit cell contains only a single HIO_3 molecule in the asymmetric unit with I-O bond lengths ranging from 1.786(5) to 1.903(7) Å. The I(V) atom is further coordinated by three oxygen atoms of neighboring acid molecules forming a distorted octahedral with a range of I-O distances (2.498(6) - 2.795(7) Å). The one structural difference that separates the β phase from the α and γ phases is that the hydroxyl group is bridging between two I(V) atoms, resulting in a smaller hydrogen bonding distance (O-O distance: 2.559 Å (β), 2.665 Å (γ) and 2.696 Å (α)) and presumably a different crystalline energy. Similar to γ-HIO_3, β-HIO_3 is metastable and slowly converts to α-HIO_3. It is hypothesized that β-HIO_3 is a transition step in the formation of α-HIO_3 and β-HIO_3 is a result of trapped water inside particles during crystallization.

Keywords

X-Ray Diffraction, Iodates, Acids, Crystal Structure, Oxides

1. Introduction

Iodine(v) oxides (*i.e.* I_2O_5, HIO_3, HI_3O_8, I_4O_9) are compounds with unique optical properties and potential for high energy release. The unique optical properties of iodine oxides, specifically iodic acid (HIO_3), are a result of the non-centrosymmetric space group $P2_12_12_1$ [1], and have led to the synthesis of different aluminum iodate species [2] [3]. Iodine oxides are also appealing for use as an oxidizer when combined with aluminum fuel particles. In fact, Smith *et al.* [4] showed detonation velocities could be achieved from aluminum iodate mixtures. The aluminum and iodine oxide reactions also have the potential to disperse high temperatures and aerosolized iodine species that can kill bacterial agents [5]. The optical properties and potential for energy release of iodine oxides are controlled by the crystalline structure of precipitated HIO_3 product [2] [3] [4].

There is only one commonly accepted polymorph for both I_2O_5 and HI_3O_8; however, there are four reported polymorphs of HIO_3 in literature: α, β, γ, and δ [1] [6] [7] [8] [9]. The most commonly reported structure of iodic acid is α-HIO_3. The γ-HIO_3 polymorph was first reported by Fischer *et al.* [1] and structurally determined by single crystal diffraction on crystals produced by mixing iodic acid with chromium. The γ-HIO_3 polymorph is thought to be a result of chromium in solution favoring the formation of dimers and trimers of HIO_3 that form γ-HIO_3 as solutions of HIO_3 and chromium precipitate. On the other hand, the β-HIO_3 polymorph was first reported in 1960 by Halasz *et al.* [8] with peak intensities determined from a powder diffraction experiment (**Table S1**); however, the diffraction pattern was not indexed. The β-HIO_3 polymorph is also mentioned briefly in Selte *et al.* [7], but is later questioned by Fischer *et al.* [1] and to our knowledge, these are the only known reports of a β polymorph of HIO_3. The δ polymorph was recently reported in Wu *et al.* [9], but detailed crystal information was not given. It is suggested that δ-HIO_3 is metastable at elevated temperatures and slow heating converts δ-HIO_3 directly into I_2O_5. The dehydration steps for the formation of HIO_3 are not well understood, but the formation of dimers, trimers and higher order polymers have been related to concentration of HIO_3 [10] [11] [12]. Many studies show polymerization of IO_3^- from solution [10] [11] [12], but a link between polymerization and formation of α-HIO_3 has not been established.

In this study, we will report on the single crystal structure of β-HIO_3 that has not previously been reported and understand the polymorphic physical behavior of β-HIO_3. To this end, the objectives were to synthesize β-HIO_3 and characterize its structure using single crystal X-ray diffraction (XRD).

2. Experimental

2.1. Sample Preparation

The synthesis method to form β-HIO_3 begins with dissolving commercially available I_2O_5 powder, supplied by Sigma Aldrich (St. Louis, MO), in distilled water. Commercial I_2O_5 was mixed to a 1:1 wt. % ratio of I_2O_5 to deionized water and placed in a beaker on a magnetic stirrer and stirred for 10 minutes at 200 RPM to allow complete I_2O_5 dissolution into solution. The iodate solution was then dried in a vent hood with an average relative humidity (RH) of 35% at 23˚C, until solid crystals precipitated from solution. Multiple samples (*i.e.*, >5) were made to establish repeatability.

2.2. Single Crystal XRD

Single crystal X-ray diffraction data were collected on a Bruker PLATFORM three circle diffractometer equipped with an APEX II CCD detector and operated at 1500 W (50 kV, 30 mA) to generate (graphite monochromated) Mo Kα radiation (λ = 0.71073 Å). Crystals were transferred from the reaction vial and placed on a glass slide in polyisobutylene. A Zeiss Stemi 305 microscope was used to identify a suitable specimen for X-ray diffraction from a representative sample of the material. The crystal and a small amount of the oil were collected on a MīTiGen cryoloop and transferred to the instrument where it was placed under a cold nitrogen stream (Oxford) maintained at 100 K throughout the duration of the experiment. The sample was optically centered with the aid of a video camera to ensure no translations were observed as the crystal was rotated through all positions.

A unit cell collection was then carried out. After it was determined that the unit cell was not present in either the CCDC or ICSD databases a sphere of data were collected. Omega scans were carried out with a 10 sec/frame exposure time and a rotation of 0.50˚ per frame. After data collection, the crystal was measured for size, morphology, and color. These values are reported in **Table S2**.

2.3. Single Crystal XRD Refinement Details

After data collection, the unit cell was re-determined using a subset of the full data collection. Intensity data were corrected for Lorentz, polarization, and background effects using the Bruker program APEX 3. A semi-empirical correction for adsorption was applied using the program SADABS [13]. The SHELXL-2014 [14], series of programs was used for the solution and refinement of the crystal structure. The hydrogen atom bound to O_1 was constrained with a DFIX command and a thermal parameter of −1.2. An extinction coefficient of 0.0298 was also applied during the final refinement.

2.4. Powder Diffraction XRD

All powder diffraction data were collected on a Rigaku Ultima III powder diffractometer. X-ray diffraction patterns were obtained by continuously scanning a 2θ range of 15˚ - 60˚, step size = 0.02˚, and scan time ranging from of 1.5 - 3 degrees/minute depending on the scan. The X-ray source was Cu Kα radiation (λ = 1.5418 Å) with an anode voltage of 40 kV and a current of 44 mA. The beam was then discriminated by Rigaku's Cross Beam parallel beam optics to create a monochromatic parallel beam. Diffraction intensities were recorded on a scintillation detector after being filtered through a Ge monochromator. Samples were prepared as standard powder mounts and diffractograms were processed through the software JADE v9.1.

3. Results

During the initial PXRD studies of what was presumed to be α-HIO_3, it was discovered that the resulting patterns did not match any indexed crystal structure. Single crystal studies were then carried out on the large blocky crystals. The β-HIO_3 phase reported in Halasz *et al.* [8] is shown in Supplemental Information. **Table S1** and is similar to the lattice parameters shown here. Because of the similarities between our results and Halasz *et al.* [8], and to avoid adding any more Greek letters to describe the phases of HIO_3, it is assumed crystals shown here are the β-HIO_3 polymorph. Since unit cell data is not reported for δ-HIO_3 in Wu *et al.* [9], only a visual comparison between β-HIO_3 and δ-HIO_3 could be made and is discussed further below. Unit Cell data, bond lengths and angles, atomic coordinates, anisotropic displacement parameters, hydrogen coordinates, and hydrogen bonds for β-HIO_3 determined by single crystal data is shown in Supplemental Information **Tables S2-S7**. While the crystal structure of β-HIO_3 was also solved in the space group α-HIO_3 ($P2_12_12_1$), it was found that the unit cell axes were all different by about 1 Å. Similar to that of α and γ phases, the unit cell contains only a single HIO_3 molecule in the asymmetric unit with I-O bond lengths ranging from 1.786(5) to 1.903(7) Å (**Table S3**). The I(V) atom is further coordinated by three oxygen atoms of neighboring acid molecules forming a distorted octahedral with a range of I-O distances (2.498(6) - 2.795(7) Å). The one structural difference, shown in **Figure 1** (e.g., α-HIO_3 shown in Supplemental Information, **Figure S1**), that separates the β phase from the α and γ phases is that the hydroxyl group is bridging between two I(V) atoms, resulting in a smaller hydrogen bonding distance (O-O distance: 2.559 Å (β), 2.665 Å (γ) and 2.696 Å (α)) and presumably a different crystalline energy.

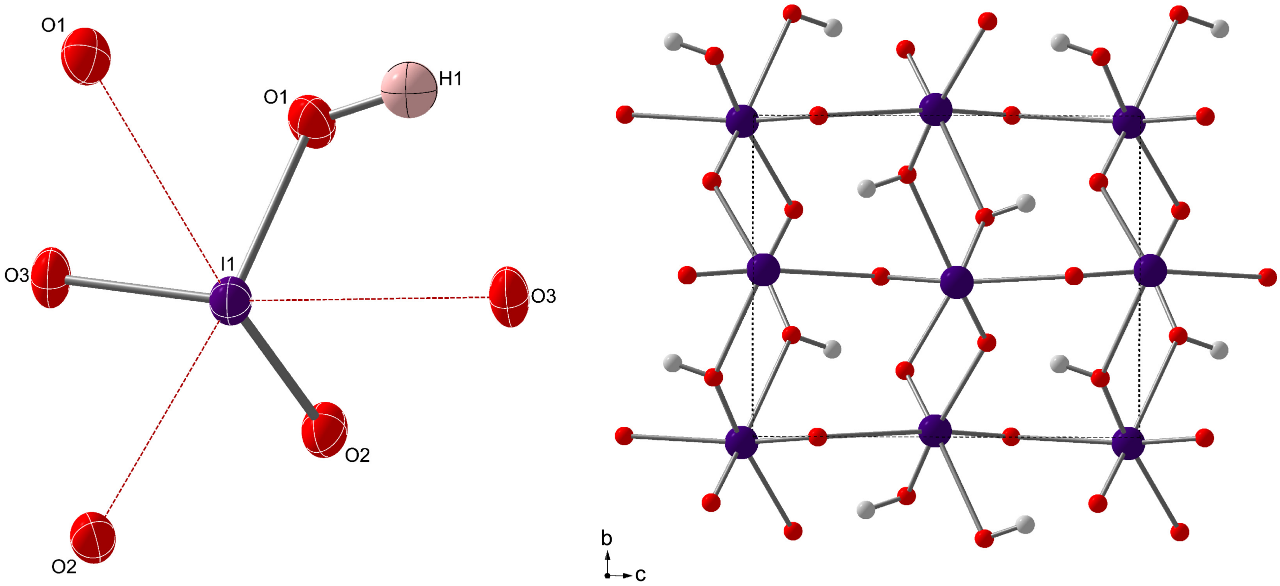

(a) (b)

Figure 1. (a) Coordination environment about the I(V) atom in β-HIO_3. The thermal ellipsoids are drawn at 50% probability level with solid and dashed lines representing short or long contacts between I and O atoms, respectively. Red, violet, and light gray ellipsoids are oxygen, iodine, and hydrogen atoms, respectively. (b) Unit cell of β-HIO_3 viewed along the axis. Red, violet, and light gray spheres represent oxygen, iodine, and hydrogen atoms, respectively.

4. Discussion

During repeatability testing, β-HIO$_3$ readily converted to α-HIO$_3$, indicating β-HIO$_3$ is metastable, similar to the γ phase. The metastable nature of β-HIO$_3$ is shown in **Figure 2**. The XRD measurements in **Figure 2** are from crystals ground into powder using mortar and pestle before data collection. In **Figure 2**, the top curve was collected immediately after drying. This sample is referred to as Sample 1 initial. The middle curve in **Figure 2** was initially ground after drying and allowed to sit in a vent hood at 20% RH for 8 days before analysis. The middle curve in **Figure 2** is pure α-HIO$_3$ and matches PDF 97-006-6643 [15] and the top curve is β-HIO$_3$. The bottom curve in **Figure 2** shows XRD measurements that were taken from Sample 1 that was put in a vent hood for 8 days prior to grinding and then ground for XRD measurements. The bottom curve in **Figure 2** shows that when Sample 1 is placed in a vent hood for 8 days as a single crystal prior to grinding and then ground for XRD measurements, it remained as β-HIO$_3$.

Figure 2 shows that β-HIO$_3$ is metastable and changes to α-HIO$_3$ over time only if the samples are ground prior to aging. Since all samples are ground before placement in the XRD, the change from β-HIO$_3$ to α-HIO$_3$ is not directly related to the physical force of the grinding and is a time dependent process related to increased surface area from grinding. It is assumed that trapped water results in the formation of β-HIO$_3$. Upon grinding, trapped water is released and drying the solid material readily converts β-HIO$_3$ into α-HIO$_3$. The validity of the assumption that trapped water results in the formation of β-HIO$_3$ is discussed below.

Figure 3 shows Sample 1 with curves from PDF #00-045-0872 labeled as $I_4O_9XH_2O$ from Wikjord *et al.* [6]. **Figure 3** shows that the sample labeled $I_4O_9XH_2O$ is β-HIO$_3$.

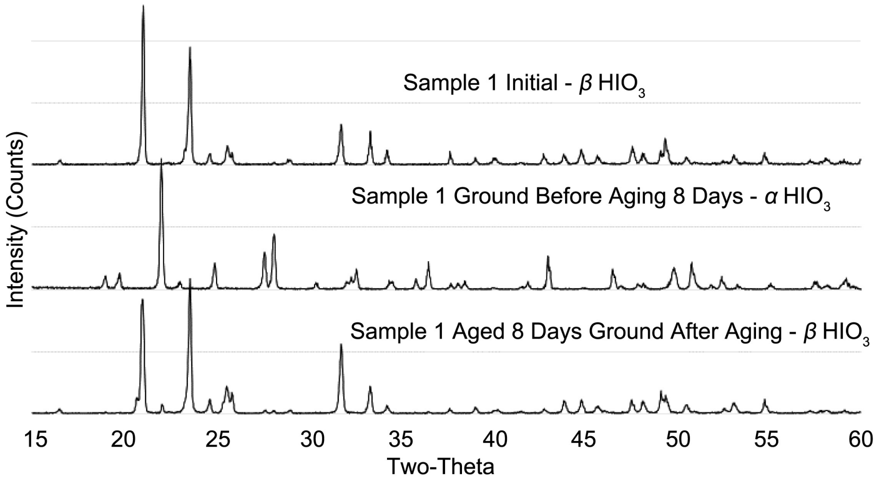

Figure 2. Three XRD scans for Sample 1 initially after drying (top scan), and Sample 1 after grinding then drying for 8 days (middle scan), Sample 1 that was dried for 8 days before grinding (bottom scan).

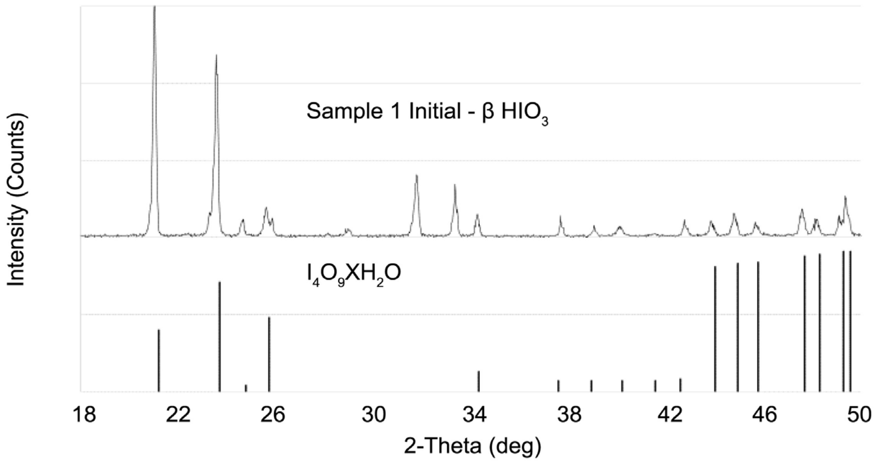

Figure 3. Diffraction pattern from XRD for Sample 1 (Black). Blue curves from PDF #00-045-0872 indicating 2-Theta and relative intensity of $I_4O_9XH_2O$.

In Wikjord *et al.* [16], the sample labeled $I_4O_9XH_2O$ was I_4O_9 hydrated by atmospheric water. In Smith *et al.* [17], it was shown that when I_4O_9 is exposed to 20% RH for 4 hours, I_4O_9 hydrates to HIO_3. Because β-HIO_3 is seen during hydration of I_4O_9 into α-HIO_3 and β-HIO_3 is seen here when I_2O_5 is mixed with water, β-HIO_3 is assumed to be a transition step in the formation of α-HIO_3. We have shown that β-HIO_3 is metastable and converts to α-HIO_3 when ground prior to aging. Because β-HIO_3 is seen during the formation of α-HIO_3 and β-HIO_3 is metastable when ground prior to aging, we propose that the formation of β-HIO_3 is an intermediate step in the formation of α-HIO_3 caused by water trapped inside the precipitated crystals.

Visual comparison of diffraction patterns between δ-HIO_3 shown in Wu *et al.* [9] and diffraction patterns shown here for β-HIO_3 are similar. Also, similar comparisons between these phases and $I_4O_9XH_2O$ have been made here and in Wu *et al.* [9], suggesting δ-HIO_3 and β-HIO_3 are the same phase. The 6 reported I-O bond distances for δ-HIO_3 are similar (less than 0.03 Å difference) to bond distances reported here for β-HIO_3. Similar bond distances and visual comparisons of diffraction patterns suggest δ-HIO_3 and β-HIO_3 are the same crystal structure. In Wu *et al.* [9], it is reported that δ-HIO_3 dehydrates directly into I_2O_5, not HI_3O_8 during slow heating conditions of DSC analysis. Because of this direct dehydration into I_2O_5 during slow heating, δ-HIO_3 is reported as metastable. This can be explained by the metastable nature of β-HIO_3 reported here and results from Smith *et al.* [18] showing that HIO_3 dehydrates directly into I_2O_5 and HI_3O_8 is formed during heating. Since comparison between measurements in Halasz *et al.* [8] and diffraction patterns obtained, using modern XRD are difficult to quantify, it is probable that δ-HIO_3 identified by Wu *et al.* [9] is actually β-HIO_3.

5. Conclusion

The β-HIO_3 polymorph, previously difficult to detect and whose existence was questioned, has been synthesized and structurally characterized. When crystals are ground before aging, β-HIO_3 is metastable and slowly converts to α-HIO_3. Experiments were designed to study the metastable nature and based on XRD analysis. β-HIO_3 may be a transition step in the formation of α-HIO_3 and result from trapped water inside HIO_3 crystals.

Acknowledgements

The authors are grateful for support from the Army Research Office under award W911NF-14-1-0250 and encouragement from our program manager, Dr. Ralph Anthenien.

References

[1] Fischer, A., and Lindsjö, M. (2005) γ-HIO_3—A Metastable, Centrosymmetric Polymorph of Iodic Acid. *Zeitschrift für anorganische und allgemeine Chemie*, **631**, 1574-1576. https://doi.org/10.1002/zaac.200500099

[2] Cradwick, P.D. and Endredy, A.S. (1977) Crystal Structure of Aluminium Iodate-Hydrogen Iodate-Water (1/1/6) and Preparation of Anhydrous Aluminium Iodate. *Journal of the Chemical Society*, **2**, 146-149.

[3] Kidyarov, B.I. (2010) Growth of Polar $Al(IO_3)_3{\cdot}8H_2O$ Crystals from Aqueous Solutions. *Bulletin of the Russian Academy of Sciences*: *Physics*, **74**, 1255-1256.

[4] Smith, D.K., Bello, M., Unruh, D.K. and Pantoya, M.L. (2017) Synthesis and Reactive Characterization of Aluminum Iodate Hexahydrate Crystals $[Al(H_2O)_6](IO_3)_3(HIO_3)_2$. *Combustion and Flame*, **179**, 154-156. https://doi.org/10.1016/j.combustflame.2017.01.012

[5] Clark, B.R. and Pantoya, M.L. (2010) The Aluminium and Iodine Pentoxide Reaction for the Destruction of Spore Forming Bacteria. *Physical Chemistry Chemical Physics*, **12**, 12653-12657. https://doi.org/10.1039/c0cp00473a

[6] Selte, K. and Kjekshus, A. (1970) Iodine Oxides Part III. The Crystal Structure of I_2O_5. *Acta Chemica Scandinavica*, **24**, 1912-1924. https://doi.org/10.3891/acta.chem.scand.24-1912

[7] Selte, K. and Kjekshus, A. (1968) Iodine Oxides Part II on the System H_2O-I_2O_5. *Acta Chemica Scandinavica*, **22**, 3309-3320. https://doi.org/10.3891/acta.chem.scand.22-3309

[8] Halasz, A., Antal, J. and Kalman, L. (1960) Jodsav Eloallitasa, Dehidratalasa Es Modosulatai. A Veszpremi Vegyipari Egyetem. *Kozlemenyei*, 159-168.

[9] Wu, T., SyBing, A., Wang, X. and Zachariah, M.R. (2017) Aerosol Synthesis of Phase Pure Iodine/Iodic Biocide Microparticles. *Journal of Materials Research*, **32**, 890-896. https://doi.org/10.1557/jmr.2017.6

[10] Pethybridge, A.D. and Prue, J. E. (1967) Equilibria in Aqueous Solutions of Iodic Acid. *Transactions of the Faraday Society*, **63**, 2019-2033. https://doi.org/10.1039/tf9676302019

[11] Goldman, S., Bates, R.G. and Robinson, R.A. (1974) Osmotic Coefficients and Activity Coefficients of Iodic Acid at High Concentrations. *Journal of Solution Chemistry*, **3**, 593-602. https://doi.org/10.1007/BF00650403

[12] Dawber, J.G. (1965) The Hammett Acidity Function in Aqueous Iodic Acid and Aqueous Periodic Acid. *Journal of the Chemical Society*, 4111-4115. https://doi.org/10.1039/jr9650004111

[13] Krause, L., Herbst-Irmer, R. and Stalke, D. (2015) An Empirical Correction for the Influence of Low-Energy Contamination. *Journal of Applied Crystallography*, **48**, 1907-1913. https://doi.org/10.1107/S1600576715020440

[14] Sheldrick, G.M. (2007) A Short History of *SHELX. Acta Crystallogr. Acta Crystallographica Section A*: *Foundations and Advances*, **A64**, 112-122. https://doi.org/10.1107/S0108767307043930

[15] Stahl, K., Svensson, C. and Szafranski, M. (1993) A Combined Neutron Powder and X-Ray Single Crystal Diffraction Study of Anhydro-Iodic Acid $DIO_3 \cdot I_2O_5$ at 293K. *Journal of Solid State Chemistry*, **102**, 408-413. https://doi.org/10.1006/jssc.1993.1052

[16] Wikjord, A., Taylor, P., Torgerson, D. and Hachkowski, L. (1980) Thermal Behaviour of Corona-Precipitated Iodine Oxides. *Thermochimica Acta*, **36**, 367-375. https://doi.org/10.1016/0040-6031(80)87032-8

[17] Smith, D.K., Pantoya, M.L., Parkey, J.S. and Kesmez, M. (2016) Reaction Kinetics and Combustion Dynamics of I_4O_9. *Journal of Visualized Experiments*, **117**, e54661.

[18] Smith, D.K., Pantoya, M.L., Parkey, J.S. and Kesmez, M. (2017) The Water-Iodine Oxide System: A Revised Mechanism for Hydration and Dehydration. *RSC Advance*, **7**, 10183-10191. https://doi.org/10.1039/C6RA27854J

Supplemental Materials

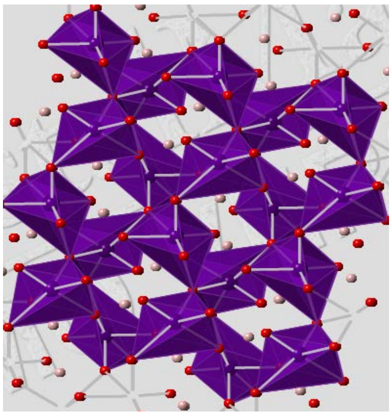

(a) Graphical representation of α-HIO_3

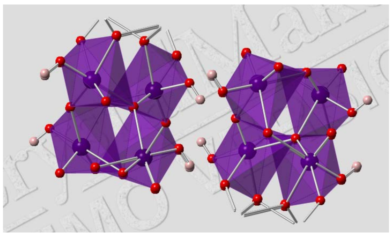

(b) Graphical representation of γ-HIO_3

Figure S1. Graphical Representation of (a) *α*-HIO_3 and (b) *γ*-HIO_3. Red, violet, and pink ellipsoids are oxygen, iodine, and hydrogen atoms, respectively.

Table S1. XRD information from Halasz *et al.*[8]

α-HIO3		β-HIO3	
I	d_{hkl}	I	d_{hkl}
10	4.071	6	4.264
5	3.557	10	3.797
9	3.160	6	3.475
6	2.746	1	3.054
4	2.575	10	2.794
5	2.452	4	2.664
5	2.342	1	2.285
3	2.168	2	2.220
5	2.092	1	2.168
4	1.939	5	2.056
3	1.886	3	1.979
9	1.823	4	1.901
9	1.789	8	1.836
3	1.713	2	1.796
3	1.663	7	1.719
4	1.594	5	1.673
6	1.562	3	1.064
		1	1.569
		2	1.541

Table S2. Unit Cell data for β-HIO_3.

HIO_3 phase	β-HIO_3
Crystal Color	colorless
Crystal Habit	block
Empirical formula	C7 H6 N2 O
Formula weight	134.14
Temperature	100(2) K
Wavelength	0.71073 A
Crystal system	Orthorombic
Space group	$P2_12_12_1$
Unit cell dimensions	a = 4.4117(8) Å, alpha = 90˚.
	b = 6.9723(13) Å, beta = 90˚.
	c = 8.4458(16) Å, gamma = 90˚.
Volume	259.79(8) $Å^3$
Z	4
Calculated density	4.498 Mg/m^3
Absorption coefficient	12.053 mm^{-1}
F(000)	312
Crystal size	0.360 × 0.350 × 0.150 mm
Theta range for data collection	3.790˚ to 27.057˚.
Limiting indices	$-5 \le h \le 5$, $-8 \le k \le 8$, $-10 \le l \le 10$
Reflections collected/unique	2921/572 [R(int) = 0.0365]
Completeness to theta = 25.242˚	100.0%
Refinement method	Full-matrix least-squares on F^2
Data/restraints/parameters	572/1/41
Goodness-of-fit on F^2	1.299
Final R indices [I > 2sigma(I)]	R1 = 0.0244, wR2 = 0.0635
R indices (all data)	R1 = 0.0244, wR2 = 0.0635
Largest diff. peak and hole	1.191 and −0.957 $e.A^{-3}$
Extinction coefficient	0.030(3)
Absolute structure parameter	−0.02(3)

Table S3. Bond lengths [Å] and angles [˚] for β-HIO_3.

Bond	Lengths(Å)	Angle(˚)
I(1)-O(3)	1.786(5)	
I(1)-O(2)	1.814(7)	
I(1)-O(1)	1.903(7)	
O(1)-H(1)	0.96(3)	
O(3)-I(1)-O(2)		100.1(3)
O(3)-I(1)-O(1)		92.2(3)
O(2)-I(1)-O(1)		94.1(3)
I(1)-O(1)-H(1)		115.0(7)

Table S4. Atomic coordinates ($\times 10^4$) and equivalent isotropic displacement parameters ($Å^2 \times 10^3$) for β-HIO_3. U(eq) is defined as one third of the trace of the orthogonalized Uij tensor.

Atom(number)	x	y	z	U(eq)
I(1)	2726(1)	4812(1)	5276(1)	17(1)
O(1)	247(14)	6842(10)	6006(7)	21(1)
O(2)	5155(15)	2939(11)	6060(7)	21(1)
O(3)	4186(13)	4989(9)	3309(6)	21(1)

Table S5. Anisotropic displacement parameters ($Å^2 \times 10^3$) for β-HIO_3. The anisotropic displacement factor exponent takes the form: $-2\pi^2 [h^2 a^{*2} U^{11} + \cdots + 2 h k a^* b^* U^{12}]$.

	U11	U22	U33	U23	U13	U12
I(1)	18(1)	18(1)	14(1)	0(1)	0(1)	0(1)
O(1)	21(3)	24(3)	18(3)	−2(2)	−3(3)	−6(3)
O(2)	25(3)	22(3)	16(3)	0(2)	1(3)	6(2)
O(3)	23(3)	29(4)	12(3)	1(3)	0(2)	−2(3)

Table S6. Hydrogen coordinates ($\times 10^4$) and isotropic displacement parameters ($Å^2 \times 10^3$) for β-HIO_3.

	x	y	z	U(eq)
H(1)	4800(200)	7280(150)	7060(50)	25

Table S7. Hydrogen bonds for β-HIO_3 where hydrogen bonds with H..A < r(A) + 2.000 Å and <DHA> 110˚ are listed.

D-H	d(D-H)	d(H..A)	<DHA	d(D..A)	A	
O1-H1	0.957	1.656	168.16	2.6	O_2	[−x + 1, y + 1/2, −z + 3/2]